Available online at www.sciencedirect.com
ScienceDirect
Trans. Nonferrous Met. Soc. China 27(2017) 1956−1963
Transactions of Nonferrous Metals Society of China
www.tnmsc.cn

Prediction model for surface layer microhardness of processed TC17 via high energy shot peening

Li-xing SUN, Miao-quan LI, Hui-min LI

School of Materials Science and Engineering, Northwestern Polytechnical University, Xi'an 710072, China

Received 31 May 2016; accepted 26 September 2016

Abstract: The bulk TC17 was subjected to the high energy shot peening (HESP) at the air pressures ranging from 0.35 to 0.55 MPa and processing durations ranging from 15 to 60 min. The microhardness ($HV_{0.02}$) from topmost surface to matrix of the HESP processed TC17 was measured, which generally decreases with the increase of depth from topmost surface to matrix and presents different variation with air pressure and processing duration at different depths. A fuzzy neural network (FNN) model was established to predict the surface layer microhardness of the HESP processed TC17, where the maximum and average difference between the measured and the predicted microhardness were respectively 8.5% and 3.2%. Applying the FNN model, the effects of the air pressure and processing duration on the microhardness at different depths were analyzed, revealing the significant interaction between the refined layer shelling and the continuous grain refinement.

Key words: TC17; high energy shot peening; microhardness; fuzzy neural network; model

1 Introduction

Nanocrystalline materials are attracting great attention due to their excellent physical, chemical and mechanical properties comparing with the conventional coarse-grained materials [1−4]. In recent years, surface severe plastic deformation has been widely used to create a nanocrystalline layer on the surface of bulk materials to achieve optimized properties on the surface compared with the unchanged underlying material. Severe plasticity roller burnishing (SPRB) [5], surface mechanical attrition treatment (SMAT) [6], supersonic fine particle bombarding (SFPB) [7], surface mechanical grinding treatment (SMGT) [8] and shot peening (SP) [9] are common methods for surface severe plastic deformation. In particular, SP is quite an effective method to fabricate ultra fine grained surface layer and significantly improve the mechanical properties in industry. High energy shot peening (HESP), i.e., SP with increased intensity and exposure duration, has been widely applied to achieving the surface nanocrystallization (SNC). UNAL and VAROL [10] found that the thickness of nanograined layer on the surface increased with the increase of plastic deformation rate in SP treatment. The grains in the surface layer of 304 stainless steel weld joint after HESP treatment were refined to a nanometer level [11]. HOU et al [12] obtained a nanocrystalline layer on the surface of AZ91D magnesium alloy via HESP, and the average grain size in the nanocrystalline layer was ~40 nm. Furthermore, the mechanical property, especially the microhardness in the processed layers, is largely increased via SNC. AHMED et al [13] found that SP markedly increased the microhardness in a small depth of deformed layer. XIE et al [14,15] pointed out that the microhardness of SP treated titanium matrix composites reached the maximum value on the topmost surface and gradually decreased with the increase of depth. Meanwhile, microhardness increased with the increase of SP intensity due to severe plastic deformation.

Artificial neural network (ANN) modelling is a non-linear statistical analysis technique. It is essentially a 'black box' linking input data to output data using a particular set of non-linear functions. ANN provides a way of using example of a target function to find the coefficients that make a certain mapping function approximate the target function as closely as possible [16]. Recently, ANN modelling is widely used to analyze non-linear and complex relationship in materials science

Foundation item: Project (51475375) supported by the National Natural Science Foundation of China
Corresponding author: Miao-quan LI; Tel: +86-29-88460328; Fax: +86-29-88492642; E-mail: honeymli@nwpu.edu.cn
DOI: 10.1016/S1003-6326(17)60220-6

and engineering [17−21]. MALINOV and SHA [22] found that the ANN model was quite convenient to investigate the effect of processing parameters on the mechanical properties of titanium alloys. KUMAR et al [23] predicted the wear behavior of SMAT treated Ti−6Al−4V by employing ANN model, in which the importance of the three input parameters in the output value was analyzed. MALEKI et al [24] established an ANN model with high accuracy to predict the mechanical properties of SP processed 18CrNiMo7-6 steel, taking the depth from topmost surface and the peening intensity as the input parameters of ANN. Fuzzy neural network (FNN) was developed based on the ANN coupling with fuzzy set, which presented higher accuracy than ANN [25,26] and was particularly suitable to handle noisy and scattered data [27].

The TC17 is a deeply hardenable near β titanium alloy, which has been widely used to fabricate the jet engine and compressor components [28]. LI et al [29] observed the gradient structure of the HESP processed TC17 and the microhardness of the surface layer increased by 43.0%. However, variation of microhardness with processing parameters (such as air pressure and processing duration) is still unclear. Therefore, the aim of this study is to achieve a comprehensive understanding of the relationship between the microhardness of the HESP processed TC17 and the processing parameters, which will contribute to optimizing the processing parameters. In the present work, a FNN model was developed to predict the surface layer microhardness of the HESP processed TC17 since the microhardness is relatively scattered. Based on the FNN model, the effects of air pressure and processing duration on the microhardness at different depths of the HESP processed TC17 were acquired. As a result, the present work can be applied to predicting the surface layer microhardness of the HESP processed TC17, which provides guidance for the better application of the SNC by the HESP in industry.

2 Experimental

2.1 Procedures

The hot-forged bar TC17 was supplied with a diameter of 50.0 mm, in which the measured chemical composition (mass fraction, %) is 5.12 Al, 2.03 Sn, 2.10 Zr, 4.04 Mo, 3.94 Cr, 0.10 Fe, 0.12 C, 0.007 N, 0.007 H, 0.12 O and balance Ti. The as-received TC17 bar was annealed at 823 K for 1 h followed by cooling in furnace to room temperature. Figure 1 shows the microstructure and XRD pattern of the annealed TC17 prior to high energy shot peening (HESP). As seen from Fig. 1, the annealed TC17 consists of primary α grains and retained transformed β phase. The TC17 specimens with dimensions of 70 mm × 19 mm × 4 mm were manufactured from the as-annealed TC17 bar, and the surfaces (70 mm × 19 mm) of TC17 specimens were ground by using silicon carbide paper to #600 prior to HESP treatment.

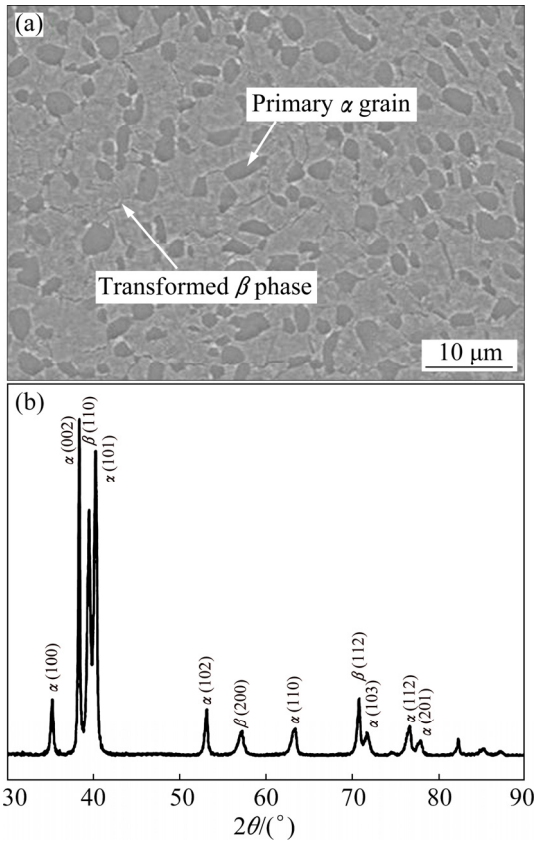

Fig. 1 Microstructure (a) and XRD pattern [29] (b) of as-annealed TC17 prior to HESP treatment

The HESP of TC17 was carried out on an air blast machine MP6000PT with a 10 mm-diameter peening nozzle. The distance between the peening nozzle and the TC17 specimen surface was 500 mm, and the mass flow rate was 10 kg/min. The surface of TC17 specimens was shot-peened by using ASH230 steel shots with a diameter of 0.6 mm at the air pressures of 0.35, 0.45, 0.55 MPa and the processing durations of 15, 30, 60 min.

Following HESP, the microhardness on the cross-section of TC17 specimen at different depths from topmost surface to matrix was measured via Tukon 2100B microhardness tester at a load of 20 g and dwell time of 10 s. Figure 2 shows the alignment of the measured points in the surface layer of the HESP processed TC17, the distance between the two neighboring points was above 30 μm and the vertical distance between the measured point and the topmost surface was measured via Leica DMI3000M optical microscope.

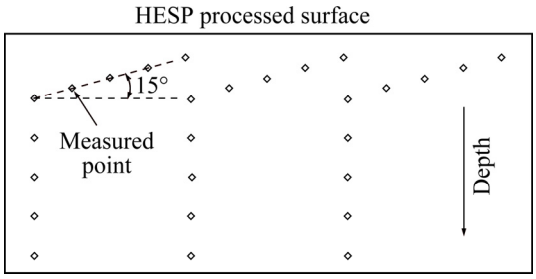

Fig. 2 Measured points of microhardness on cross section of HESP processed TC17

2.2 Microhardness

Figure 3 shows the microhardness variation of the HESP processed TC17 with the depth below topmost surface. In general, the microhardness gradually decreases with the increase of depth from topmost surface to matrix, and tends to be steady at a depth of ~100 μm below topmost surface (Fig. 3). However, the effect of air pressure and processing duration on the microhardness seems to be different at different depths below topmost surface. As a result, it is quite difficult to determine the effect of the air pressure and processing duration on the microhardness based on the scattered microhardness in Fig. 3.

3 Establishment of fuzzy neural network model

3.1 FNN model

Figure 4 presents the fuzzy neural network (FNN) model structure for predicting the microhardness ($HV_{0.02}$) of high energy shot peening (HESP) processed TC17. The air pressure (p) processing duration (t) and depth below topmost surface (h) are the three inputs, and the microhardness (M) is the output of network. US, UM, and UL represent the membership functions, q_0^i, q_1^i, q_2^i, q_3^i are the weight coefficients of the middle layer of network, S and Q respectively represent the sum and multiplication, w^i is the weight value representing the ith rule degree, and m^i is the outputs of middle layer [30].

The activation function in the output layer of FNN model is a linear function, while the activation function in the hidden layer is selected to be a sigmoidal function

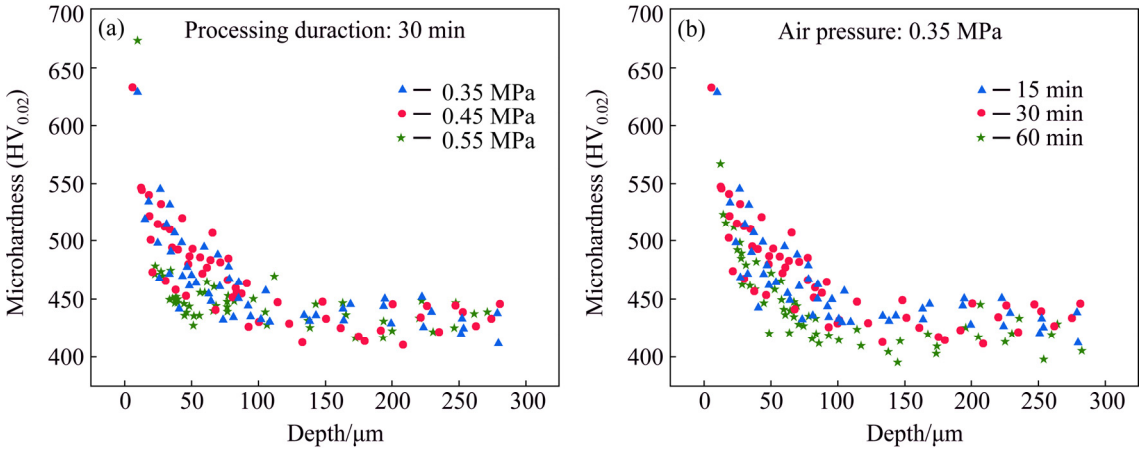

Fig. 3 Variation of microhardness with depth below topmost surface of HESP processed TC17

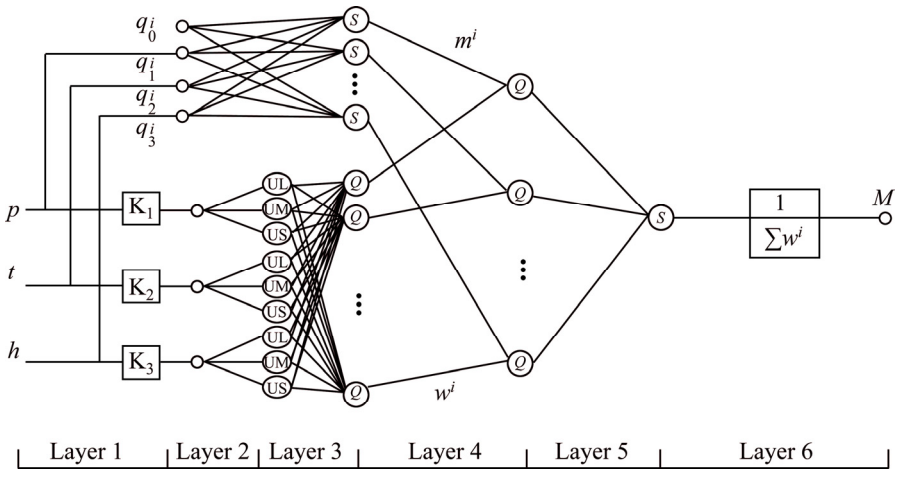

Fig. 4 FNN model for predicting microhardness of HESP processed TC17

as follows:

$$\mu_j^i = \exp[-(x_j - a_j^i)^2 / b_j^i], \quad j=1,\ 2,\ 3 \tag{1}$$

where x_1, x_2, x_3 respectively represent the air pressure, processing duration, depth below topmost surface, a_j^i and b_j^i are the material constants.

The fuzzy subset of process parameters with large {UL}, middle {UM}, and small {US} is regulated and shown in Fig. 5, and the subject functions are covered as follows:

For air pressure in Fig. 5(a),

$$\mathrm{UL}_1(x) = \begin{cases} 1, & p \geq 0.55 \\ \exp\left[\dfrac{-(p-0.55)^2}{1.06}\right], & p < 0.55 \end{cases} \tag{2}$$

$$\mathrm{UM}_1(x) = \exp\left[\frac{-(p-0.45)^2}{0.16}\right] \tag{3}$$

$$\mathrm{US}_1(x) = \begin{cases} 1, & p \leq 0.35 \\ \exp\left[\dfrac{-(p-0.35)^2}{1.06}\right], & p > 0.35 \end{cases} \tag{4}$$

For processing duration in Fig. 5(b),

$$\mathrm{UL}_2(x) = \begin{cases} 1, & t \geq 60 \\ \exp\left[\dfrac{-(t-60)^2}{1210}\right], & t < 60 \end{cases} \tag{5}$$

$$\mathrm{UM}_2(x) = \exp\left[\frac{-(t-37.5)^2}{601}\right] \tag{6}$$

$$\mathrm{US}_2(x) = \begin{cases} 1, & t \leq 15 \\ \exp\left[\dfrac{-(t-15)^2}{1210}\right], & t > 15 \end{cases} \tag{7}$$

For depth below topmost surface in Fig. 5(c),

$$\mathrm{UL}_3(x) = \begin{cases} 1, & h \geq 151 \\ \exp\left[\dfrac{-(h-151)^2}{205}\right], & h < 151 \end{cases} \tag{8}$$

$$\mathrm{UM}_3(x) = \exp\left[\frac{-(h-78.5)^2}{33}\right] \tag{9}$$

$$\mathrm{US}_3(x) = \begin{cases} 1, & h \leq 6 \\ \exp\left[\dfrac{-(h-6)^2}{205}\right], & h > 6 \end{cases} \tag{10}$$

The total 27 fuzzy rules can be acquired as follows:

For the rule R^i,

If p is UL_1, t is UL_2 and h is UL_3, then,

$$m^i = q_0^i + q_1^i \cdot p + q_2^i \cdot t + q_3^i \cdot h \tag{11}$$

$$w^i = \mu_1^i \cdot \mu_2^i \cdot \mu_3^i \tag{12}$$

The total output (M) of the Pi-Sigma FNN model is as follows:

$$M = \sum_{i=1}^{27} w^i m^i \Big/ \sum_{i=1}^{27} w^i = \sum_{i=1}^{27} \frac{\mu_1^i(p) \cdot \mu_2^i(t) \cdot \mu_3^i(h) \cdot \left(q_0^i + q_1^i \cdot p + q_2^i \cdot t + q_3^i \cdot h\right)}{\mu_1^i(p) \cdot \mu_2^i(t) \cdot \mu_3^i(h)} \tag{13}$$

To optimize the variables of membership functions and weight coefficients in FNN model, an error back-propagation learning algorithm is presented by minimizing the error function as follows:

$$E = \frac{1}{2}(m_\mathrm{d} - M)^2 \tag{14}$$

where m_d is the desired output, and M is the current output of network.

Updating the weight and threshold as follows:

$$q_j^i(k+1) = q_j^i(k) - \eta(m_\mathrm{d} - M) \cdot w^i \Big/ \sum_{i=1}^{27} w^i \cdot x_j^i, \quad j=1,\ 2,\ 3 \tag{15}$$

$$a_j^i(k+1) = a_j^i(k) - \beta(m_\mathrm{d} - M) \cdot \left[m^i \sum_{i=1}^{27} w^i - \sum_{i=1}^{27} w^i m_j^i \right] \cdot 2 \cdot \left(x_j - a_j^i\right) w^i \Big/ \left[b_j^i \left(\sum_{i=1}^{27} w^i \right)^2 \right], \quad j=1,\ 2,\ 3 \tag{16}$$

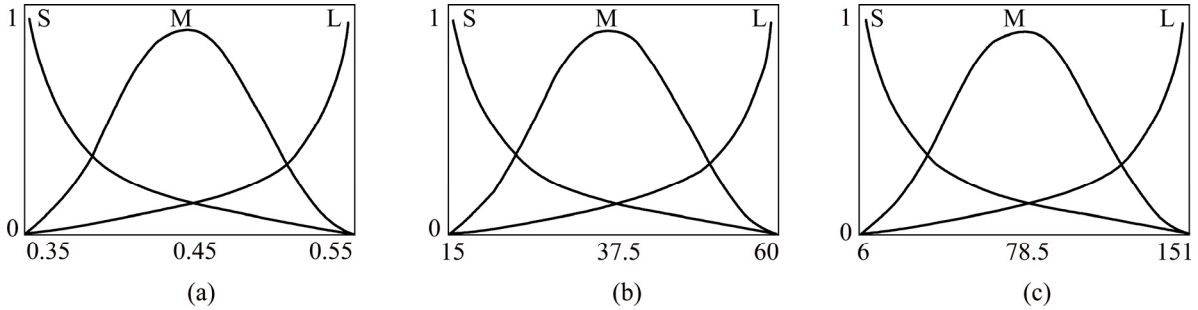

Fig. 5 Parted sections of fuzzy set for processing parameters of air pressure (a), processing duration (b) and depth below topmost surface (c)

$$b_j^i(k+1)=b_j^i(k)-\beta(m_{\mathrm{d}}-M)\cdot\left[m^i\sum_{i=1}^{27}w^i-\sum_{i=1}^{27}w^i m_j^i\right]\cdot\left(x_j-a_j^i\right)^2 w^i\Bigg/\left[\left(b_j^i\right)^2\left(\sum_{i=1}^{27}w^i\right)^2\right],\ j=1,\ 2,\ 3 \quad (17)$$

where k is the number of weight updates, η and β are the learning rates.

3.2 Prediction of microhardness

In the present work, 160 data points of the measured microhardness at the air pressures ranging from 0.35 to 0.55 MPa, the processing durations ranging from 15 to 60 min and the depths from 6 to 151 μm below topmost surface are selected as the teacher's samples to train the FNN model. The other 25 data points are the verification samples and all the verification samples are within the teacher's bounds. In the training process, the learning rates η and β in FNN model are 6.6×10^{-5} and 2.8×10^{-5}, respectively. It should be noted that the back-propagation learning algorithm is iterative, numerous re-initialization and re-training of the network were established to achieve the best solution. The maximum difference and the average difference between the predicted and the experimental microhardnesses of the teacher's samples are 9.3% and 2.8% after 5294 repetition training cycles.

3.3 Verification of FNN model

The comparison between the verification data and the predicted microhardness of the HESP processed TC17 by using FNN model is shown in Table 1. As seen from Table 1, the maximum difference and the average error between the predicted and the measured microhardness values are 8.5% and 3.2%, respectively. As a result, it could be concluded that the present FNN model can be used to efficiently predict the surface layer microhardness of HESP processed TC17.

4 Effect of processing parameter on microhardness

By using the fuzzy neural network (FNN) model, the effect of the air pressure and processing duration on the surface layer microhardness of high energy shot peening (HESP) processed TC17 is acquired. The typical predicted results are shown in Fig. 6 and Fig. 7.

Figure 6 shows the microhardness variation of predicted surface layer of HESP processed TC17 with the depth below topmost surface. As seen from Fig. 6, a gradient change occurs in the surface layer microhardness of HESP processed TC17. Our previous work [29] demonstrated that gradient nanocrystalline structure of TC17 was attained via HESP, where severe plastic deformation with high strain and strain rate causes rapid accumulation of dislocations at the topmost surface layer of HESP processed TC17. Consequently, significant work-hardening occurs [31]. The refinement of grains highly increases the grain boundary density and the microhardness. With the increase of depth below topmost surface, the grain size gradually tends towards that of the matrix and the dislocation density decreases. Consequently, microhardness decreases rapidly and then tends to be a steady value at about 100 μm below topmost surface.

Table 1 Comparison between predicted microhardness of HESP processed TC17 and verification data

No.	Air pressure/ MPa	Processing duration/ min	Depth/ μm	Microhardness ($HV_{0.02}$)		Error/ %
				Measured	FNN	
1	0.45	30	13	546	576	5.5
2	0.35	15	14	539	570	5.8
3	0.45	30	21	483	524	8.5
4	0.35	30	25	499	510	2.2
5	0.35	15	25	520	511	1.7
6	0.35	60	28	489	487	0.4
7	0.35	15	29	488	496	1.6
8	0.35	15	33	507	486	4.1
9	0.55	30	33	450	454	0.9
10	0.45	30	43	520	492	5.4
11	0.55	30	44	446	431	3.4
12	0.35	60	59	449	441	1.8
13	0.45	30	66	477	441	7.5
14	0.35	30	71	461	464	0.7
15	0.55	30	78	454	444	2.2
16	0.45	30	82	451	446	1.1
17	0.35	60	83	433	424	2.1
18	0.35	15	89	453	465	2.6
19	0.35	30	94	434	455	4.8
20	0.45	30	100	430	435	1.2
21	0.35	15	103	428	437	2.1
22	0.35	30	105	457	443	3.1
23	0.55	30	107	427	455	6.6
24	0.35	15	134	421	431	2.4
25	0.35	60	144	395	409	3.5

Figure 7 shows the microhardness variation with air pressure and processing duration at different depths below topmost surface of HESP processed TC17. As seen from Fig. 7(a), the microhardness at 10 μm below topmost surface increases with the increase of processing duration and then decreases at the processing duration above 25 min. The microhardness at the depths of 30 and

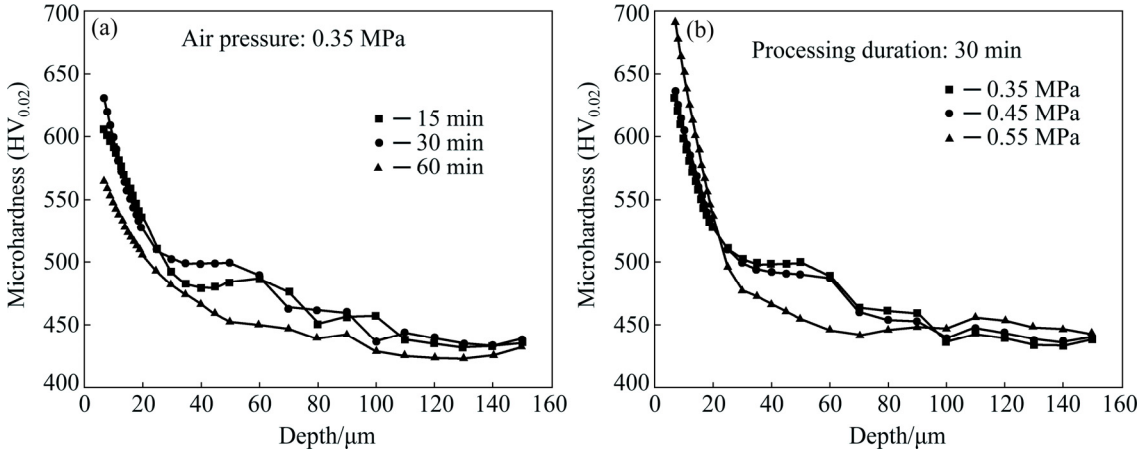

Fig. 6 Variation of predicted microhardness with depth below topmost surface of HESP processed TC17

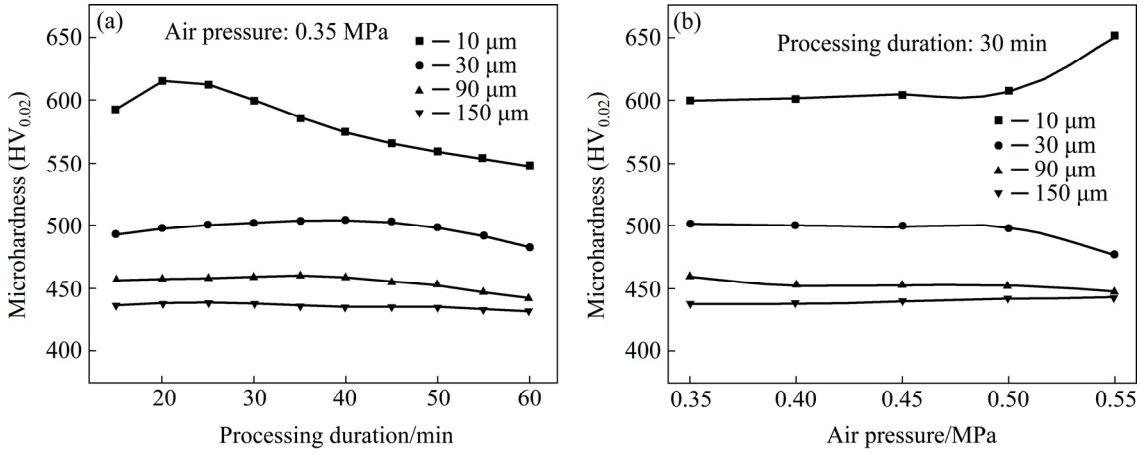

Fig. 7 Effects of processing duration (a) and air pressure (b) on microhardness at different surface layer depths of HESP processed TC17

90 μm below topmost surface slightly increases and then decreases at the processing duration above 40 min. The microhardness at a depth of 150 μm below topmost surface slightly varies with the increase of processing duration. As seen from Fig. 7(b), with the increase of air pressure, the microhardness at 10 μm below topmost surface slightly increases until a sharp increase at a pressure of 0.5 MPa. The microhardnesses at 30 μm and 90 μm below topmost surface gradually decrease with the increase of air pressure. Similarly as that in Fig. 7(a), the microhardness at a depth of 150 μm below topmost surface slightly varies with the increase of air pressure.

For HESP, grain refinement until nanocrystallization needs duration accumulation. Consequently, the microhardness at 10 μm below topmost surface increases as the processing duration increases from 15 to 25 min (Fig. 7(a)) due to continuous grain refinement effect. However, with the further increase of processing duration, the refined layer at the topmost surface gradually peels off because of the severe plastic deformation. That is, the nanocrystallized topmost surface is replaced by the newly exposed layer with larger grain size. As a result, the microhardness at 10 μm below topmost surface decreases at the processing duration above 25 min, as shown in Fig. 7(a). It should be noted that a steep near-surface gradient structure of the HESP processed TC17 occurs followed by a smooth variation as depth increases. That is, the effect of the topmost layer shelling on the microhardness decreases as the depth below topmost surface increases. Therefore, the microhardness slightly increases due to gradually formed refinement layer and then decreases at the processing duration above 40 min at the depths of 30 and 90 μm below topmost surface (Fig. 7(a)). On the other hand, the refined layer shells at a high rate as the air pressure increases, and the high air pressure greatly accelerates the grain size refinement. As a result, as the air pressure increase to 0.5 MPa, the microhardness slightly increases where the refined layer shelling and the grain size refinement are almost in equilibrium. With the further increase of air pressure, the grain size refinement caused by high air pressure plays a more significant role.

Finally, a sharp increase of microhardness at 10 μm below topmost surface occurs, as shown in Fig. 7(b). At the processing duration above 30 min, the peeling off of topmost layer occurs and the new duration accumulation begins, which can be confirmed as shown in Fig. 7(a). Consequently, the grain refinement at the depths of 30 and 90 μm below topmost surface decreases and further refinement is not sufficient, leading to a gradual decrease in microhardness with the increase of air pressure, as shown in Fig. 7(b). At 150 μm below topmost surface, the effects of the processing parameters on the microhardness are slight, therefore, the microhardness slightly varies with the increase of processing duration and air pressure (Figs. 7(a) and (b)).

5 Conclusions

1) The surface layer microhardness of the HESP processed TC17 generally shows a gradient variation with the depth below topmost surface to matrix, and the microhardness shows different variations with air pressure and processing duration at different depths.

2) The FNN model for predicting the surface layer microhardness of the HESP processed TC17 is established. By using the FNN model, the maximum and the average difference between the predicted and measured microhardnesses are 8.5% and 3.2%, respectively.

3) Applying the FNN model, effect of the air pressure and processing duration on the surface layer microhardness of HESP processed TC17 was analyzed. The microhardness at 10 μm below topmost surface shows an initial increase and then decreases following duration above 25 min, and increases with the increase of air pressure. The microhardnesses at 30 μm and 90 μm below topmost surface slightly increase and then decrease at the processing duration above 40 min, and gradually decrease with the increase of air pressure. The microhardness at 150 μm below topmost surface slightly varies with the increase of air pressure and processing duration.

References

[1] GLEITER H. Nanocrystalline materials [J]. Progress in Materials Science, 1989, 33: 223−315.

[2] KUMAR K S, SWYGENHOVEN H V, SURESH S. Mechanical behavior of nanocrystalline metals and alloys [J]. Acta Materialia, 2003, 51: 5743−5774.

[3] RAJABI M, SEDIGHI R M, RABIEE S M. Thermal stability of nanocrystalline Mg-based alloys prepared via mechanical alloying [J]. Transactions of Nonferrous Metals Society of China, 2016, 26: 398−405.

[4] MAO Xiang-yang, LI Dong-yang, WANG Zhang-zhong, ZHAO Xiu-ming, CAI Lu. Surface nanocrystallization by mechanical punching process for improving microstructure and properties of Cu−30Ni alloy [J]. Transactions of Nonferrous Metals Society of China, 2013, 23: 1694−1700.

[5] ZHAO Jing, XIA Wei, LI Ning, LI Feng-lei. A gradient nano/micro-structured surface layer on copper induced by severe plasticity roller burnishing [J]. Transactions of Nonferrous Metals Society of China, 2014, 24: 441−448.

[6] JIN Lei, CUI Wen-fang, SONG Xiu, LIU Gang, ZHOU Lian. Effects of surface nanocrystallization on corrosion resistance of β-type titanium alloy [J]. Transactions of Nonferrous Metals Society of China, 2014, 24: 2529−2538.

[7] GE Li-ling, TIAN Na, LU Zheng-xin, YOU Cai-yin. Influence of the surface nanocrystallization on the gas nitriding of Ti−6Al−4V alloy [J]. Applied Surface Science, 2013, 286: 412−416.

[8] YIN Yan-fei, XU Wei, SUN Qiao-yan, XIAO Lin, SUN Jun. Deformation and fracture behavior of commercially pure titanium with gradient nano-to-micron-grained surface layer [J]. Transactions of Nonferrous Metals Society of China, 2015, 25: 738−747.

[9] LIU Yin-gang, LI Hui-ming, LI Miao-quan. Characterization of surface layer in TC17 alloy treated by air blast shot peening [J]. Materials Design, 2015, 65: 120−126.

[10] UNAL O, VAROL R. Surface severe plastic deformation of AISI 304 via conventional shot peening, severe shot peening and repeening [J]. Applied Surface Science, 2015, 351: 289−295.

[11] LU Zhi-ming, SHI Lai-min, ZHU Shen-jin, TANG Zhi-dong, JIANG Ya-zhou. Effect of high energy shot peening pressure on the stress corrosion cracking of the weld joint of 304 austenitic stainless steel [J]. Materials Science and Engineering A, 2015, 637: 170−174.

[12] HOU Li-feng, WEI Ying-hui, LIU Bao-sheng, XU Bing-she. Microstructure evolution of AZ91D induced by high energy shot peening [J]. Transactions of Nonferrous Metals Society of China, 2008, 18: 1053−1057.

[13] AHMED A A, MHAEDE M, BASHA M, WOLLMANN M, WAGNER L. Effect of micro shot peening on the mechanical properties and corrosion behavior of two microstructure Ti−6Al−4V alloy [J]. Applied Surface Science, 2016, 363: 50−58.

[14] XIE Le-chun, JIANG Chuan-hai, LU Wei-jie, ZHAN Ke, CHEN Yan-hua. Investigation on the residual stress and microstructure of (TiB+TiC)/Ti−6Al−4V composite after shot peening [J]. Materials Science and Engineering A, 2011, 528: 3423−3427.

[15] XIE Le-chun, WEN Yan, ZHAN Ke, WANG Li-qiang, JIANG Chuan-hai, JI V. Characterization on surface mechanical properties of Ti−6Al−4V after shot peening [J]. Journal of Alloys and Compounds, 2016, 666: 65−70.

[16] GUO Z, SHA W. Modelling the correlation between processing parameters and properties of maraging steels using artificial neural network [J]. Computational Materials Science, 2004, 29: 12−28.

[17] KHALAJ G, POURALIAKBAR H. Computer-aided modeling for predicting layer thickness of a duplex treated ceramic coating on tool steels [J]. Ceramics International, 2014, 40: 5515−5522.

[18] POURALIAKBAR H, KHALAJ G, JANDAGHI M R, KHALAJ M J. Study on the correlation of toughness with chemical composition and tensile test results in microalloyed API pipeline steels [J]. Journal of Mining and Metallurgy, Section B: Metallurgy, 2015, 51: 173−178.

[19] POURALIAKBAR H, KHALAJ G, GOMIDZELOVIC L, KHALAJ M J, NAZERFAKHARI M. Duplex ceramic coating produced by low temperature thermo-reactive deposition and diffusion on the cold work tool steel substrate: Thermodynamics, kinetics and modeling [J]. Ceramics International, 2015, 41: 9350−9360.

[20] POURALIAKBAR H, KHALAJ M J, NAZERFAKHARI M, KHALAJ G. Artificial neural networks for hardness prediction of HAZ with chemical composition and tensile test of X70 pipeline steels [J]. Journal of Iron and Steel Research International, 2015, 22: 446−450.

[21] KHALAJ G, KHALAJ M J. Application of ANFIS for modeling of

layer thickness of chromium carbonitride coating [J]. Neural Computing and Applications, 2014, 24: 685−694.
[22] MALINOV S, SHA W. Application of artificial neural networks for modelling correlations in titanium alloys [J]. Materials Science and Engineering A, 2004, 365: 202−211.
[23] KUMAR S A, RAMAN S G S, NARAYANAN T S N S, GNANAMOORTHY R. Prediction of fretting wear behavior of surface mechanical attrition treated Ti−6Al−4V using artificial neural network [J]. Materials and Design, 2013, 49: 992−999.
[24] MALEKI E, SHERAFATNIA K. Investigation of single and dual step shot peening effects on mechanical and metallurgical properties of 18CrNiMo7-6 Steel using artificial neural network [J]. International Journal of Materials, Mechanics and Manufacturing, 2016, 4: 100−105.
[25] LI Miao-quan, CHEN Dun-jun, XIONG Ai-ming, LONG Li. An adaptive prediction model of grain size for the forging of Ti−6Al−4V alloy based on fuzzy neural networks [J]. Journal of Materials Processing Technology, 2002, 123: 377−381.
[26] YU Wei-xin, LI Miao-quan, LUO Jiao, SU Shao-bo, LI Chang-qing. Prediction of the mechanical properties of the post-forged Ti−6Al−4V alloy using fuzzy neural network [J]. Materials and Design, 2010, 31: 3282−3288.
[27] SUN Li-xing, LI Miao-quan. FNN model for carbide size of M50 steel during hot deformation [J]. Ironmaking and Steelmaking, 2016, 43: 220−227.
[28] BOYER R R. An overview on the use of titanium in the aerospace industry [J]. Materials Science and Engineering A, 1996, 213: 103−114.
[29] LI Hui-min, LIU Yin-gang, LI Miao-quan, LIU Hong-jie. The gradient crystalline structure and microhardness in the treated layer of TC17 via high energy shot peening [J]. Applied Surface Science, 2015, 357: 197−203.
[30] LI Miao-quan, ZHANG Xun-yin. Modeling of the microstructure variables in the isothermal compression of TC11 alloy using fuzzy neural networks [J]. Materials Science and Engineering A, 2011, 528: 2265−2270.
[31] HUMPHREYS F J, HATHERLY M. Recrystallization and related annealing phenomena [M]. 2nd ed. Amsterdam: Elsevier, 2004.

高能喷丸处理后 TC17 合金表层显微硬度预测模型

孙利星, 李淼泉, 李慧敏

西北工业大学 材料学院, 西安 710072

摘 要：通过高能喷丸对 TC17 合金进行表面处理，喷丸空气压力为 0.35~0.55 MPa，喷丸时间为 15~60 min。测量了 TC17 合金高能喷丸处理后最表层至基体的显微硬度。测量结果表明，显微硬度随深度的增大而逐渐减小，且不同深度处显微硬度随空气压力与喷丸时间的变化各不相同。建立了 TC17 合金高能喷丸处理后表层显微硬度的模糊神经网络模型。借助该模型，显微硬度的预测值与测量值的最大相对误差为 8.5%，平均误差为 3.2%。基于模糊神经网络模型，研究了空气压力与喷丸时间对 TC17 合金高能喷丸处理后不同深度处显微硬度的影响。结果表明，细化层的脱落与连续的晶粒细化作用之间有显著的交互作用。

关键词：TC17 合金；高能喷丸；显微硬度；模糊神经网络；模型

(Edited by Xiang-qun LI)